

THE UBIQUITY OF COEVAL STARBURSTS IN MASSIVE GALAXY CLUSTER PROGENITORS

CAITLIN M. CASEY

Department of Astronomy, The University of Texas at Austin, 2515 Speedway Blvd Stop C1400, Austin, TX 78712, USA
 Draft version April 6, 2018

ABSTRACT

The Universe’s largest galaxy clusters likely built the majority of their massive $>10^{11} M_{\odot}$ galaxies in simultaneous, short-lived bursts of activity well before virialization. This conclusion is reached from emerging datasets on $z > 2$ proto-clusters and the characteristics of their member galaxies, in particular, rare starbursts and ultraluminous active galactic nuclei (AGN). The most challenging observational hurdle in identifying such structures is their very large volumes, $\sim 10^4$ comoving Mpc^3 at $z > 2$, subtending areas \sim half a degree on the sky. Thus the contrast afforded by an overabundance of very rare galaxies in comparison to the background can more easily distinguish overdense structures from the surrounding, normal density field. Five $2 \lesssim z \lesssim 3$ proto-clusters from the literature are discussed in detail and are found to contain up to 12 dusty starbursts or luminous AGN galaxies each, a phenomenon that is unlikely to occur by chance even in overdense environments. These are contrasted with three higher-redshift ($4 \lesssim z \lesssim 5.5$) dusty star-forming galaxy (DSFG) groups, whose evolutionary fate is less clear. Measurements of DSFGs’ gas depletion times suggest that they are indeed short-lived on ~ 100 Myr timescales, and accordingly the probability of finding a structure containing more than 8 such systems is $\sim 0.2\%$, unless their ‘triggering’ is correlated on very large spatial scales, ~ 10 Mpc across. The volume density of DSFG-rich proto-clusters is found to be comparable to all $>10^{15} M_{\odot}$ galaxy clusters in the nearby Universe, a factor of five larger than expected in some simulations. Some tension yet exists between measurements of the volume density of DSFG-rich proto-clusters and the expectation that they are generated via short-lived episodes, as the latter suggests only a fraction ($< \frac{1}{2}$) of all proto-clusters should be rich with DSFGs. However, improved observations of proto-clusters over large regions of sky will certainly shed more light on the assembly of galaxy clusters, and whether or not they build their galaxies through episodic bursts as suggested here.

Subject headings: galaxy clusters – galaxies: high-redshift – galaxies: infrared – active galactic nuclei

1. INTRODUCTION

The environmental dependence of galaxies’ evolution is observationally elusive. Locally, it is clear that galaxies residing in the most massive environments exhibit characteristics markedly different from their counterparts in the field: they are more massive (e.g. Collins *et al.* 2009; van der Burg *et al.* 2013), they are forming relatively few stars (Balogh *et al.* 1998; Lewis *et al.* 2002), they are preferentially red (Wake *et al.* 2005), and they lack spiral structure (Skibba *et al.* 2009). At their cores, hot inter-cluster gas—containing $\sim 90\%$ of the cluster’s baryonic matter—renders these massive systems easy to detect via their emission of Bremsstrahlung radiation in the X-ray (see review of Kravtsov & Borgani 2012). These threads of observational evidence, combined with knowledge of density fluctuations in the early Universe imprinted on the Cosmic Microwave Background (Sheth, Mo & Tormen 2001), have formed the backbone of our understanding of hierarchical growth in galaxy formation (Springel 2005; Vogelsberger *et al.* 2014). Higher density environments saw accelerated evolution by forming most of their galaxies early and coalescing at earlier times. What does this imply for observations of overdense environments at high-redshift?

In line with hierarchical expectation, some works have observed a reversal of the star-formation-density relation at $z \sim 1$ (Elbaz *et al.* 2007; Cooper *et al.* 2008), whereby

galaxies in overdense environments at high-redshift are *more* likely to be star-forming than field galaxies or similar-mass galaxies in overdensities in the local Universe. However, several other works do not see this reversal (Patel *et al.* 2009; Cucciati *et al.* 2010; Bolzonella *et al.* 2010; Scoville *et al.* 2013), leading to some uncertainty in the processes driving evolution of clusters at early times.

Observations of clusters in the early Universe ($z > 1$) themselves also have considerable potential as tools for testing galaxy formation theory in a cosmological context and placing independent constraints on fundamental cosmological parameters. For example, discovering a single cluster of sufficient mass at $z \geq 2$ ($M_{\text{halo}} \sim 5 \times 10^{14} M_{\odot}$) can place significant constraints on current cosmological models (e.g. Harrison & Coles 2012), just as the discovery of a population of early massive galaxies may already challenge that paradigm (Steinhardt *et al.* 2015). Hence, several observational efforts to identify high-redshift overdensities have been pursued over the past few decades (Subramanian & Swarup 1992; Steidel *et al.* 1998, 2005; Ivison *et al.* 2000; Stevens *et al.* 2003; Miley *et al.* 2004; Doherty *et al.* 2010; Noble *et al.* 2013; Rigby *et al.* 2014; Clements *et al.* 2014; Planck Collaboration *et al.* 2015).

Unfortunately, detecting galaxy clusters at $z > 2$ has proved especially challenging. While X-ray searches are efficient at selecting massive clusters through emission of hot gas at $z \lesssim 1.5$ (e.g. Rosati, Borgani & Norman 2002),

the rapid surface brightness dimming of X-ray emission makes it an inefficient observable at high-redshift. Other techniques for identifying cluster environments are similarly limited to $z \lesssim 2$, such as optical searches for the galaxy red sequence, which demonstrates the presence of an evolved galaxy population (Gladders & Yee 2000; Brodwin *et al.* 2007; Eisenhardt *et al.* 2008; Andreon *et al.* 2014; Newman *et al.* 2014), and identifications made using the Sunyaev-Zel'dovich effect (Menanteau & Hughes 2009; Vanderlinde *et al.* 2010; Planck Collaboration *et al.* 2013). In addition to the difficulty in making these observations at high-redshift, it is perhaps not surprising that these methods struggle since they are optimized to detect *evolved* clusters with older (red, massive, elliptical) galaxy populations or the signature of a hot inter-cluster medium (ICM). At sufficiently early times, cluster environments may not have yet virialized to the point where the ICM heats, implying that detection in the X-rays or S-Z are not optimal techniques, even if the sensitivity were substantially deep to reach overdensities at those epochs.

Despite the difficulty in identifying clusters at high-redshift, about twenty overdensities have been observationally identified and spectroscopically confirmed at $z > 2$. The primary identification technique has been targeted narrow-band filter searches around single rare galaxies with spectroscopic redshifts (e.g. Venemans *et al.* 2007). These narrow band imaging campaigns focus on detection of Ly α (Lyman- α emitters, LAEs, Shimasaku *et al.* 2003; Palunas *et al.* 2004; Venemans *et al.* 2002, 2005; Kuiper *et al.* 2011) or H α (H α emitters, HAEs, Doherty *et al.* 2010; Hatch *et al.* 2011; Tanaka *et al.* 2011; Hayashi *et al.* 2012; Koyama *et al.* 2013) at the redshift of the quasar or radio galaxy. Typically an excess of candidate emission line galaxies is found in the vicinity of the targeted rare source when compared against the field. While this constitutes strong evidence for highly clustered overdensities, most of the emission line sources lack full spectral information or multiwavelength characterization.

In contrast, some overdensities have been serendipitously found through large spectroscopic campaigns (Steidel *et al.* 1998, 2005). Though rare, these constitute the most spectroscopically complete proto-clusters, some with over 100 identified LBGs or LAE member galaxies extending several Mpc on a side. A further handful of proto-clusters with 5–40 LBG members have been identified surrounding single bright submillimeter galaxies, or dusty star-forming galaxies (DSFGs, at $z = 2 - 5.3$ Chapman *et al.* 2009; Carilli *et al.* 2011; Capak *et al.* 2011; Walter *et al.* 2012; Casey *et al.* 2015).

While the range of high- z overdensities are diverse, this paper focuses only on those that are spectroscopically confirmed with an excess of DSFGs and luminous AGN. These structures are of particular interest as they provide unique testbeds for understanding the assembly history of massive clusters by virtue of the presumed rarity and short lifetimes of their constituents (Solomon & Sage 1988; Bothwell *et al.* 2013; Carilli & Walter 2013; Martini 2004). § 2 presents the observational characteristics of these DSFG/AGN-rich structures. Their potential to collapse into some of the Universe’s most massive clusters is addressed in § 3, and their unique constraints on galaxy cluster assembly is discussed in § 4. Predictions

are made for the next generation of large observational surveys and large-box simulations in § 5, with conclusions given in § 6. Throughout, a Λ CDM cosmology is assumed with $H_0 = 71 \text{ km s}^{-1} \text{ Mpc}^{-1}$ and $\Omega_m = 0.27$ (Hinshaw *et al.* 2009), and comoving Mpc is denoted throughout as cMpc to distinguish from proper Mpc.

2. DSFG/AGN-RICH PROTO-CLUSTERS

Here I present the existing observational characteristics for overdense structures at $z \gtrsim 2$ with robust spectroscopic redshifts and an overabundance of DSFGs or luminous AGN. The importance of an overabundance of DSFGs or luminous AGN is key: these are types of galaxies that are $\gtrsim 100$ times more rare than most ‘normal’ L_\star galaxies across all epochs. Their rarity is what makes them useful for studying high-redshift overdensities, not only because they represent a potentially critical evolutionary stage for early massive galaxy formation (Toft *et al.* 2014), but also because a group of them in close proximity is exceedingly rare and can easily identify an overdense structure too large to be identified through more common galaxy populations. Furthermore, as will be discussed in later sections, they can place unique constraints on the assembly history of proto-clusters.

Their star-formation rates, dark matter halo masses, structure volumes, and respective population overdensities are estimated below and discussed in context of each proto-cluster’s observations. The star-formation rates are computed with careful treatment of individual dust-obscured starbursts, which will dominate the calculation of SFR, as well as a rough constraint on the contribution from other optically-selected members like LBGs. Dark matter halo masses are estimated using abundance matching techniques (Behroozi, Wechsler & Conroy 2013), requiring estimates to each individual member’s stellar mass, unless stated otherwise. Due to shear numbers, the halo mass is dominated by optically-identified member galaxies. Third, any available information on the physical extent of the structure is summarized, e.g. its occupied volume, although the uncertainty of such an estimation should be emphasized. Due to spectroscopic incompleteness, all of these estimates may be viewed as lower limits in physical terms, but can be regarded as representative of existing observable constraints.

Galaxy overdensities are quantified with the measurement of $\delta_{\text{gal}} = (N_{\text{gal}} - N_{\text{exp}})/N_{\text{exp}}$, where N_{gal} is the observed number of member galaxies and N_{exp} is the expected number of galaxies in the same volume of blank field, or expected cosmic density. The expected number of galaxies is determined using known luminosity functions for ‘normal’ galaxies like LBGs (e.g. Reddy & Steidel 2009; van der Burg, Hildebrandt & Erben 2010), X-ray AGN (Silverman *et al.* 2008) and DSFGs (Casey, Narayanan & Cooray 2014). Different survey depths of different fields are taken into account in determining how prevalent a given population may be. The observational characteristics of all proto-clusters, as discussed in this section, are summarized in Table 1.

2.1. GOODS-N Structure at $z = 1.99$

Blain *et al.* (2004) and Chapman *et al.* (2009) identified a particularly DSFG-rich proto-cluster at $z = 1.99$ in the Hubble Deep Field North. The structure contains

TABLE 1
AGGREGATE MASS, SFR, AND VOLUME CHARACTERISTICS OF HIGH- z DSFG-RICH PROTO-CLUSTERS

NAME	z	N_{gals}	δ_{gals}	N_{rare}	δ_{rare}	REF.	TOTAL STELLAR MASS [M_{\odot}]	HALO MASS (at z) [M_{\odot}]	VOLUME [cMpc^3]	TOTAL SFR [$M_{\odot} \text{ yr}^{-1}$]
Genuine DSFG-rich Proto-clusters:										
GOODS-N proto-cluster	1.99	34	2.5	11	10	3, 5	6.5×10^{11}	$(6 \pm 3) \times 10^{13}$	9000	2600 ± 300
COSMOS $z = 2.10$ proto-cluster	2.10	~ 100	8	10	13	13, 19	1.9×10^{12}	$(1.7 \pm 1.2) \times 10^{14}$	15000	5300 ± 600
MRC 1138–256 proto-cluster	2.16	~ 80	12	5	12	2, 10, 14	$\sim 1 \times 10^{12}$	$\sim 1 \times 10^{14}$	8000	2200 ± 500
COSMOS $z = 2.47$ proto-cluster	2.47	57	3.3	12	10	15, 16, 17	1.0×10^{12}	$(8 \pm 3) \times 10^{13}$	15000	4500 ± 500
SSA22 proto-cluster	3.09	~ 280	39	12	10	1, 4, 7, 8, 18	–	$(8 \pm 4) \times 10^{13}$	21000	5700 ± 800
Other identified DSFG-rich Overdensities:										
GN20 overdensity	4.05	8	–	3	> 100	6, 12	2.8×10^{11}	$(2 \pm 0.4) \times 10^{12}$	–**	1500 ± 800
HDF 850.1 overdensity	5.18	13	3.6	2	6	11	–	$> 1.3 \times 10^{11}$	20000	850 ± 300
AzTEC-3 overdensity	5.30	11	30	2	80	9	$\sim 2 \times 10^{10}$	$\sim 4 \times 10^{11}$	$\gtrsim 500$	1600 ± 500

Table Notes. References are 1=Steidel *et al.* (1998), 2=Kurk *et al.* (2000), 3=Blain *et al.* (2004), 4=Hayashino *et al.* (2004), 5=Chapman *et al.* (2009), 6=Daddi *et al.* (2009), 7=Tamura *et al.* (2009), 8=Lehmer *et al.* (2009), 9=Capak *et al.* (2011), 10=Kuiper *et al.* (2011), 11=Walter *et al.* (2012), 12=Hodge *et al.* (2013), 13=Yuan *et al.* (2014), 14=Dannerbauer *et al.* (2014), 15=Casey *et al.* (2015), 16=Diener *et al.* (2015), 17=Chiang *et al.* (2015), 18=Umehata *et al.* (2015), and 19=Hung *et al.*, submitted.

** The GN20 structure is notably small as an association of 3 galaxies (or a total of 8, including candidates); the estimation of its occupied volume is thus quite uncertain.

TABLE 2
OBSERVED CHARACTERISTICS OF HIGH- z DSFG-RICH PROTO-CLUSTERS

NAME	z	POSITION	SOLID ANGLE [deg^2]	GALAXY DENSITY [deg^{-2}]
GOODS-N proto-cluster	1.99	12:36:30+62:13:00	$0.17^{\circ} \times 0.17^{\circ}$	1200
COSMOS $z = 2.10$ proto-cluster	2.10	10:00:23+02:15:07	$0.34^{\circ} \times 0.13^{\circ}$	2300
MRC 1138–256 proto-cluster	2.16	11:40:48–26:28:00	$0.20^{\circ} \times 0.10^{\circ}$	4000
COSMOS $z = 2.47$ proto-cluster	2.47	10:00:31+02:22:22	$0.33^{\circ} \times 0.42^{\circ}$	400
SSA22 proto-cluster	3.09	22:17:34+00:15:01	$0.33^{\circ} \times 0.50^{\circ}$	1700
GN20 overdensity	4.05	12:37:11+62:22:05	$0.01^{\circ} \times 0.01^{\circ}$	600
HDF 850.1 overdensity	5.18	12:36:52+62:12:26	$0.10^{\circ} \times 0.13^{\circ}$	1000
AzTEC-3 overdensity	5.30	10:00:20+02:35:20	$0.003^{\circ} \times 0.003^{\circ}$	1.2×10^6

Table Notes. Positions and observed ‘‘sizes’’ of high- z DSFG-rich proto-clusters. Note the large variation in proto-cluster solid angle and confirmed galaxy density (i.e. number of galaxies belonging to the proto-cluster in its solid angle). It is likely that these sizes and perceived galaxy densities are limited by observational selection effects and are not representative of the structures’ true physical characteristics.

at least 24 optically selected, spectroscopically confirmed members in addition to eleven rare types of galaxies spanning the entire GOODS-N field of view (four submillimeter galaxies, ten radio galaxies, and six X-ray galaxies, all of which have substantial overlap). While Chapman *et al.* (2009) present potentially as many as nine DSFGs, a few of those are spurious spikes in the original SCUBA maps and others only bright radio galaxies (Amy Barger, private communication).

Using deep data in HDF and more recent collections of deep submillimeter data from *Herschel* (Oliver *et al.* 2012) and SCUBA-2 (Chen *et al.* 2013), I re-derive far-infrared SEDs for this GOODS-N structure’s DSFGs using a simple modified black body and powerlaw prescription (Casey 2012). The modified black body dominates the SED fit at rest-frame wavelengths $\gtrsim 40 \mu\text{m}$, and the mid-infrared powerlaw dominates from $5 \lesssim \lambda \lesssim 40 \mu\text{m}$. Note that the calculation of star-formation rates is largely insensitive to far-infrared SED fitting technique, as differences in methods are typically much less than measurement uncertainty (see § 4.2 of Casey, Narayanan & Cooray 2014). The far-infrared photometry is provided in Table 3. Stellar masses and star-formation rates for non-DSFG members are determined via detailed optical and near-infrared SED fitting with MAG-

PHYS (da Cunha, Charlot & Elbaz 2008) to rest-frame UV data through *Spitzer* IRAC available in GOODS-N (Capak *et al.* 2004). The median stellar mass for non-DSFG members is $6 \times 10^9 M_{\odot}$ and the median SFR is $20 M_{\odot} \text{ yr}^{-1}$. The total stellar mass for identified cluster members is $6.5 \times 10^{11} M_{\odot}$ and the total star-formation rate is $2600 \pm 300 M_{\odot} \text{ yr}^{-1}$. The aggregate star-formation rate is dominated (88%) by the DSFGs, as is the stellar mass total (70%).

The stellar masses of the GOODS-N proto-cluster members can be checked by extrapolating *Spitzer* IRAC photometry to rest-frame $1.6 \mu\text{m}$ (Hainline *et al.* 2009), as is done in Chapman *et al.* (2009). Although the star-formation histories of DSFGs are quite uncertain, and this compounds in the assumed mass-to-light ratio, I apply a $L_{\text{H}}/M_{\star} = 7.9^{+0.8}_{-2.1} L_{\odot}/\text{mag}$ (Hainline *et al.* 2011) for DSFGs and LBGs alike and derive a total integrated stellar mass of $1.3 \times 10^{12} M_{\odot}$, within a factor of two of the SED estimate. Treating each galaxy as its own halo (which is appropriate given the spatial distribution of such structures), a total dark matter halo mass is inferred for the proto-cluster of $(6 \pm 3) \times 10^{13} M_{\odot}$ at $z = 1.99$. Assuming an exponential growth in line with large box simulations (Wechsler *et al.* 2002), this proto-cluster would grow to a mass of $(9 \pm 5) \times 10^{14}$ at $z = 0$.

TABLE 3
FIR PHOTOMETRIC CHARACTERISTICS OF DSFGs IN THE HDF $z = 1.99$ STRUCTURE

NAME	z	ALT NAME [◇]	S_{250} [mJy]	S_{350} [mJy]	S_{500} [mJy]	S_{850} [mJy]	$S_{1.4}$ [μ Jy]	L_{IR} [L_{\odot}]	SFR [$M_{\odot} \text{ yr}^{-1}$]	REF.
DSFG J123600.13+621047.2	1.994	SMG-93	—	12.9 \pm 4.9	13.1 \pm 4.5	7.9 \pm 2.4*	128.5 \pm 8.1	(1.1 $^{+1.0}_{-0.5}$) $\times 10^{12}$	100 $^{+170}_{-90}$	1
DSFG J123618.32+621550.5	1.994	SMG132	22.9 \pm 4.5	30.0 \pm 5.3	24.8 \pm 5.4	7.3 \pm 1.1	172.0 \pm 8.4	(3.5 $^{+1.2}_{-0.9}$) $\times 10^{12}$	330 $^{+210}_{-150}$	1,4
DSFG J123621.25+621708.3	1.988	†SMG140e+w	25.1 \pm 4.5	19.8 \pm 4.9	7.5 \pm 4.8	7.8 \pm 1.9	169.4 \pm 8.8	(3.3 $^{+1.8}_{-1.2}$) $\times 10^{12}$	310 $^{+310}_{-210}$	1
DSFG J123635.57+621424.0	2.001	SMG172	21.1 \pm 4.5	11.0 \pm 5.0	—	5.5 \pm 1.4	77.0 \pm 7.8	(2.8 $^{+1.8}_{-1.0}$) $\times 10^{12}$	260 $^{+310}_{-170}$	1
DSFG J123711.99+621325.6	1.992	SMG255	14.9 \pm 4.5	13.1 \pm 5.0	—	4.2 \pm 1.4	50.2 \pm 8.1	(2.0 $^{+1.8}_{-1.0}$) $\times 10^{12}$	190 $^{+310}_{-170}$	1, 2, 4
DSFG J123711.32+621330.9	1.993	SFRG254	38.0 \pm 4.5	34.7 \pm 5.0	25.0 \pm 5.0	—	79.6 \pm 17.2	(5.7 $^{+3.8}_{-2.3}$) $\times 10^{12}$	540 $^{+650}_{-400}$	1, 2, 4
RAD J123632.53+620759.8	1.993	SMG169	—	—	—	5.5 \pm 1.3*	80.4 \pm 8.6	(3.9 $^{+1.3}_{-0.3}$) $\times 10^{11}$	40 $^{+30}_{-5}$	1
RAD J123617.54+621540.7	1.993	‡SFRG130	—	—	—	—	200.0 \pm 12.8	—	<12	1, 3
RAD J123640.73+621011.0	1.977	SFRG179	—	—	—	—	72.5 \pm 8.3	—	<50	1

Table Notes. References noted in the last column are 1=Chapman *et al.* (2009), 2=Casey *et al.* (2009), 3=Casey *et al.* (2009), 4=Bothwell *et al.* (2010).

[◇] ALT NAME is the alternate name used for this source throughout the literature, and as stated in Chapman *et al.* (2009).

* The original 850 μ m flux densities as measured by SCUBA for SMG-93 and SMG169 are inconsistent with more recent 850 μ m follow-up with SCUBA-2 (Chen *et al.* 2013).

† Source SMG140e+w is a double radio source within a single SCUBA beam; the second radio source has flux density 63.4 \pm 10.6 μ Jy.

‡ Source SMG130 was originally thought to be a submillimeter-faint star-forming radio galaxy (SFRG/OFRG) in Chapman *et al.* (2004) but was later revealed through high-resolution radio imaging to be a low-luminosity AGN in an evolved galaxy (Casey *et al.* 2009).

The comoving volume is calculated within a $10' \times 10'$ area and approximate redshift bounds of $1.982 < z < 2.010$ as 9000 cMpc^3 . Most of this is along the line of sight, as the spatial coverage for deep spectra does not extend significantly beyond the deep GOODS-N *HST* coverage. It would be surprising if this structure is not extended spatially beyond the limited field-of-view of the GOODS-N pencil-beam survey.

2.2. COSMOS structure at $z = 2.10$

Yuan *et al.* (2014) identify a Virgo-like progenitor in the COSMOS field at $z = 2.095$ with 57 spectroscopic members with a cluster velocity dispersion measured to be $\sigma = 552 \pm 52 \text{ km s}^{-1}$. The proto-cluster was revealed through spectroscopic follow-up of a zFOURGE candidate cluster at $z = 2.2$ identified with photometric techniques by Spitler *et al.* (2012), and they predict a halo mass at $z \sim 0$ of $10^{14.4 \pm 0.3} M_{\odot}$.

Through our own Keck MOSFIRE programs to follow-up SCUBA-2 and *Herschel*-selected DSFGs in the COSMOS field, there are seven spectroscopically-identified DSFGs coincident with this structure, four of which are published in Casey *et al.* (2012). The details of this proto-cluster, its remaining DSFGs and AGN of which there are ten total, will be discussed in more detail in Hung *et al.*, submitted. The DSFGs reach well beyond the original bounds of the structure identified in Yuan *et al.* (2014), and an LBG overdensity exists across $\sim 30'$ scales from zCOSMOS samples (Lilly *et al.* 2009). The DSFG overdensity, centered at $z = 2.10$, is measured to be $\delta_{\text{DSFG}} = 13$, with a corresponding LBG overdensity (measured from zCOSMOS) of $\delta_{\text{LBG}} = 8$.

The extensive 30+ bands of imaging in the COSMOS field are used to infer stellar masses and star-formation rates from SEDs with MAGPHYS, all the details of which will be given in Hung *et al.* The aggregate stellar mass for these sources is $1.9 \times 10^{12} M_{\odot}$ and star-formation rate is $5300 \pm 600 M_{\odot} \text{ yr}^{-1}$. A lower limit on the volume for this structure is placed at 15000 cMpc^3 , using a sky area coverage of $8' \times 20'$. While one of the DSFGs lies sig-

nificantly outside of this area, and could easily justify a doubling of the volume, spectroscopic incompleteness in that patch of sky significantly limits our ability to assess the structure's extent.

2.3. MRC1138–256, or the “Spiderweb Galaxy” structure at $z = 2.16$

This structure was originally characterized in Kurk *et al.* (2000) and has a number of candidate LAEs in addition to HAEs. The most notable member is the ‘Spiderweb Galaxy’ described by Kuiper *et al.* (2011), a radio-loud starburst with luminous AGN and giant Ly α halo. Dannerbauer *et al.* (2014) present submillimeter data of the area, and point to a number of identified DSFGs that could reside within the structure. From their work, five DSFGs have secure spectroscopic confirmation within a much more spatially compact region.

The stellar masses of these DSFGs are estimated in Dannerbauer *et al.* (2014), averaging around $10^{11} M_{\odot}$. Lacking stellar mass estimates on the other spectroscopically identified proto-cluster members, the aggregate stellar mass can be estimated roughly at $\sim 1 \times 10^{12} M_{\odot}$ and inferred halo mass of $1 \times 10^{14} M_{\odot}$ if abundance matching is used to separately scale to halo mass. This is perhaps less appropriate in this structure than in the others given the compact spatial arrangement. It is possible that the mass surrounding the identified DSFGs in this sub-halo has virialized. Further observations will be crucial to interpreting the size and mass of this structure (Kurk *et al.*, in prep) and how it compares to the other high- z structures in the literature.

Without detailed SED information on each proto-cluster member, it is not possible to directly derive a total star-formation rate to the system. However, given the far-infrared photometry provided in Dannerbauer *et al.* (2014), the SFR estimates are re-derived in a self-consistent way, and arrive at $2200 \pm 500 M_{\odot} \text{ yr}^{-1}$ as the total for the structure. Note that this may be overestimated due to lack of correction for confusion boosting on the far-infrared photometry, but may be an underes-

timate due to lack of inclusion of all proto-cluster members.

The volume estimate of 3000 cMpc^3 for the structure surrounding MRC1138–256 uses a sky area roughly $6' \times 9'$ with a redshift interval $2.154 < z < 2.171$. Like the GOODS-N structure, MRC1138–256 is limited by a narrow field of view for multiwavelength follow-up, and so all estimated parameters should be regarded as lower limits, perhaps only representative of a smaller sub-halo in a larger overdensity.

2.4. COSMOS structure at $z = 2.47$

Casey *et al.* (2015) describe an extended structure in the COSMOS field at $z = 2.47$ which contains seven spectroscopically-confirmed DSFGs, and five additional AGN. The large-field coverage of COSMOS is uniquely useful in the identification of this overdensity, as the LBG excess is only moderate on smaller scales ($< 1'$). Intriguingly, a few other works identify a neighboring overdensity of LAEs (Diener *et al.* 2015; Chiang *et al.* 2015) at $z = 2.44 - 2.45$. While this LAE-rich structure is offset both spatially and in redshift, by $\sim 50 \text{ cMpc}$, it could be associated as part of a colossally-large overdensity. Lee *et al.* (2016) detect this $z = 2.44 - 2.45$ structure using absorption of neutral hydrogen in the IGM, though existing data is limited to the coincident spatial region and does not cover the $z \sim 2.47$ DSFG-rich structure. More work is currently being carried out to determine the possible filamentary connection between the two, and if this also relates to a possible overdensity of DSFGs detected at $z = 2.51 - 2.55$ in the same field. Note that the number of galaxies in this structure has increased since its initial publication in Casey *et al.* (2015); the public release of results from the VIMOS Ultra Deep Survey (VUDS) in February 2016 revealed an additional 15 previously unidentified, spectroscopically-confirmed proto-cluster members.

The detailed calculation of this structure’s net star-formation rate of $4500 \pm 500 \text{ M}_\odot \text{ yr}^{-1}$, total stellar mass of 1.0×10^{12} , halo mass of $(8 \pm 3) \times 10^{13}$, and volume of 15000 cMpc^3 is given in Casey *et al.* (2015) and is calculated in a fully consistent way with the other structures described in this paper.

2.5. SSA22 $z = 3.09$ Structure

The SSA22 structure was originally revealed in Steidel *et al.* (1998) as one of the first high- z proto-clusters ever detected in LBGs, and as such is probably one of the best-studied proto-clusters in the literature. Narrow-band Ly α follow-up has revealed an extended excess of $z = 3.1$ LAEs extending as far as 60 Mpc comoving (Hayashino *et al.* 2004; Yamada *et al.* 2012; Matsuda *et al.* 2005). The full extent of the structure is shown in Hayashino *et al.* (2004) in LAEs as reaching over three distinct filaments about $20' \times 3'$, $10' \times 4'$ and $8' \times 8'$ across; the implied volume in the redshift range $3.07 < z < 3.11$ is $\approx 21000 \text{ cMpc}^3$.

The structure is also home to an excess of DSFGs (Tamura *et al.* 2009). Three DSFGs were spectroscopically confirmed as proto-cluster members in Chapman *et al.* (2005), a further three were identified as Ly α emitters with submillimeter detections in Geach *et al.* (2005), and most recently some ALMA-detected submillimeter

sources have spectroscopic confirmations from the node of the proto-cluster (Kubo *et al.* 2015; Umehata *et al.* 2015). Four of these sources are significantly fainter than the other eight, and so are excluded from the DSFG-overdensity calculation though are still considered for their bulk contributions to SFR. The FIR characteristics of these twelve DSFGs are given in Table 4. Extrapolating from the $850 \mu\text{m}$ and 1.1 mm flux density and a 35 K modified blackbody template, the SFRs measured for SSA22 DSFGs ranges from $120 - 1400 \text{ M}_\odot \text{ yr}^{-1}$ and totals $5670 \text{ M}_\odot \text{ yr}^{-1}$. In addition, there are twelve X-ray luminous AGN present in the proto-cluster (Lehmer *et al.* 2009), four of which overlap with the DSFGs, bringing the total rare galaxy count to 13. Lehmer *et al.* (2009) also finds evidence that the LBGs in SSA22 are a bit more massive (by factors of 1.2–1.8) than LBGs in the field, and Hine *et al.* (2016) shows evidence for enhanced merger rates in proto-cluster member galaxies.

It is difficult to precisely identify how many spectroscopically confirmed proto-cluster members sit in the SSA22 proto-cluster. The original spectroscopic sample has only 16 members, while the narrow-band follow-up imaging around Ly α has 283 confident candidates extending \sim half a degree across the sky. In addition, there have been several further spectroscopic campaigns in the field, confirming a handful of interesting sources. No stellar mass estimates are given for this structure, although Steidel *et al.* (1998) do provide an estimate of the total halo mass of $(8 \pm 4) \times 10^{13} \text{ M}_\odot$ computed using the implied bias from the LBG overdensity.

2.6. The GN20 overdensity at $z = 4.05$

One of the brightest submillimeter galaxies from the original SCUBA surveys, GN20 eluded redshift identification for many years until Daddi *et al.* (2009) confirmed it at $z = 4.055$ through a serendipitous CO detection. Follow-up work revealed two accompanying galaxies, themselves submillimeter emitters, at the same redshift. This GN20 system is discussed in detail in Hodge *et al.* (2013). This overdensity is significantly different than the structures discussed so far, with far fewer proto-cluster members identified through spectroscopy. This may indicate that it is intrinsically less massive than the other structures, or that spectroscopic incompleteness is quite severe. Because the structure sits in the well studied GOODS-N field (like the GOODS-N structure at $z = 1.99$) spectroscopic incompleteness is less likely, particularly at a redshift where detecting Ly α emitters would be fairly straightforward with ground-based optical multi-object spectrographs (Wirth *et al.* 2004; Cowie *et al.* 2004).

Stellar mass estimates for this group are given in Daddi *et al.* (2009) and Hodge *et al.* (2013) for the three DSFGs: GN20, GN20.2a, and GN20.2b. The sum of their stellar masses is $\sim 3 \times 10^{11} \text{ M}_\odot$, and total star-formation rate of $1500 \pm 800 \text{ M}_\odot \text{ yr}^{-1}$. Hodge *et al.* reveal six tentative CO(2-1) detections surrounding the GN20 complex, and the 50 cMpc^3 volume for the structure is thus estimated within a $4' \times 3'$ area and a redshift interval of $\Delta z = 0.0014$ at $z = 4.055$. Like the lack of large numbers of spectroscopic confirmations, the estimated volume is quite a bit smaller than the other structures presented here, which may be due to the fact that we are looking at

TABLE 4
FIR CHARACTERISTICS OF DSFGs IN THE SSA22 $z = 3.09$ STRUCTURE

NAME	z	S_{850} [mJy]	$S_{1.1\text{mm}}$ [mJy]	L_{IR} [L_{\odot}]	SFR [$M_{\odot} \text{ yr}^{-1}$]	X-ray AGN	REF.
DSFG J221732.41+001743.8	3.092	...	6.4±0.2	$(1.1^{+0.9}_{-0.5}) \times 10^{13}$	1000^{+800}_{-500}	Y	3
DSFG J221735.15+001537.3	3.096/8	6.3±1.3	2.3±0.1	$(4.5^{+3.7}_{-2.0}) \times 10^{12}$	420^{+340}_{-190}	N	1, 3
DSFG J221735.83+001559.0	3.089	4.9±1.3	1.8±0.1	$(3.5^{+2.9}_{-1.6}) \times 10^{12}$	330^{+270}_{-150}	Y	1, 3
DSFG J221732.01+001655.4	3.091	3.2±1.6	0.7±0.1	$(1.8^{+1.4}_{-0.8}) \times 10^{12}$	160^{+140}_{-70}	Y	2, 3
DSFG J221725.97+001238.9	3.102	17.4±2.9	–	$(1.4^{+1.2}_{-0.6}) \times 10^{13}$	1400^{+1100}_{-600}	N	1, 2
LAB J221711.67+001644.9	3.06–3.13	5.2±1.4	–	$(4.3^{+3.5}_{-1.9}) \times 10^{12}$	400^{+330}_{-180}	N	2
LAB J221802.27+002556.9	3.06–3.13	6.1±1.4	–	$(5.1^{+4.1}_{-2.3}) \times 10^{12}$	480^{+390}_{-210}	N	2
LAB J221728.90+000751.0	3.06–3.13	11.0±1.5	–	$(9.1^{+7.3}_{-4.1}) \times 10^{12}$	860^{+700}_{-390}	N	2
†DSFG J221737.11+001712.4	3.090	...	1.1±0.1	$(1.8^{+1.5}_{-0.8}) \times 10^{12}$	170^{+140}_{-80}	N	3
†DSFG J221736.54+001622.7	3.095	...	1.0±0.1	$(1.7^{+1.4}_{-0.7}) \times 10^{12}$	160^{+130}_{-70}	Y	3
†DSFG J221737.05+001822.4	3.086	...	1.1±0.1	$(1.8^{+1.5}_{-0.8}) \times 10^{12}$	170^{+140}_{-80}	N	3
†DSFG J221736.81+001818.1	3.085	...	0.8±0.2	$(1.3^{+1.1}_{-0.6}) \times 10^{12}$	120^{+100}_{-60}	N	3

Table Notes. Sources with † preceding the name are not included in the calculation of SSA22’s rare object overdensity, δ_{rare} , as they are much lower luminosities than the other DSFGs in the sample, detected over much larger areas. References are 1=Chapman *et al.* (2005), 2=Geach *et al.* (2005), 3=Umehata *et al.* (2015). 850 μm flux densities are taken from Chapman *et al.* (2005) and Geach *et al.* (2005) while 1.1 mm flux densities from ALMA are given in Umehata *et al.* (2015). Note that 850 μm coverage extends over a much larger area than the ‘ALMA Deep Field’ of the SSA22 proto-cluster node but with shallower depth. The redshifts of the three LAEs are not precisely known as they were identified through narrow-band imaging and not direct spectroscopic observations. The X-ray AGN column indicates whether or not the given DSFG is matched to an X-ray source in Lehmer *et al.* (2009). Total infrared luminosities and star-formation rates are derived by assuming a 35 K dust modified blackbody plus mid-infrared powerlaw.

a sub-halo in a larger structure, or more likely, a group which is intrinsically less massive than the five structures presented so far that sit at lower redshift.

2.7. The HDF 850.1 overdensity at $z = 5.18$

Walter *et al.* (2012) describes the massive starbursting submillimeter galaxy HDF 850.1 and the structure surrounding it at $z \approx 5.2$. Like GN20, HDF 850.1 eluded redshift confirmation for over a decade and was only confirmed via detection of molecular gas. While it is the only DSFG in this $z = 5.2$ overdensity, there is an accompanying QSO and eleven other spectroscopically-confirmed galaxies at the same redshift. This overdensity extends across a large filamentary area $10' \times 30'$. Its total star formation rate is estimated just using the single submillimeter source for lack of adequate photometric constraints on the other proto-cluster members, at $850 \pm 300 M_{\odot} \text{ yr}^{-1}$. Similarly, given the high redshift of this structure, stellar masses are unconstrained due to lack of atmospheric transmission around rest-frame $1.6 \mu\text{m}$. Do note, however, that there is a dynamical mass constraint on the galaxy HDF 850.1 of $(1.3 \pm 0.4) \times 10^{11} M_{\odot}$, which can be used as a lower limit to the halo mass of the system at $z \approx 5.2$. The volume estimate of 20000 cMpc^3 is derived assuming the above solid angle and a redshift range of $5.183 < z < 5.213$.

2.8. The AzTEC-3 overdensity at $z = 5.30$

Capak *et al.* (2011) report the discovery of an overdensity surrounding the interesting luminous DSFG named AzTEC-3 in the COSMOS field. Within a $1'$ diameter region, there appear to be twelve proto-cluster members at $z \approx 5.3$, including the single DSFG AzTEC-3 and one X-ray detected quasar at a distance of 13 Mpc from the starburst. Similar to the HDF 850.1 overdensity, estimating stellar masses for these sources is quite challenging, although Capak *et al.* (2011) offer this computation directly, totaling $> 2 \times 10^{10} M_{\odot}$. They extrapolate this to

a halo mass using abundance matching techniques and estimate a lower limit of $> 4 \times 10^{11} M_{\odot}$. The total SFR estimate is again taken for the sole DSFG member at $1600 \pm 500 M_{\odot} \text{ yr}^{-1}$. The volume of the structure is estimated within a $0.5'$ radius and a $\Delta z = 0.03$ interval, arriving at a lower limit of $\gtrsim 500 \text{ cMpc}^3$. As is the case with the other high-redshift overdensities, it is important to stress that the AzTEC-3 system could be the progenitor of a less massive overdensity.

2.9. Candidate DSFG-rich Proto-clusters

It is important to emphasize again that a number of candidate high- z , DSFG-rich proto-clusters have recently been found thanks to wide-area surveys like those from *Planck* and *Herschel* but are awaiting spectroscopic confirmation (Clements *et al.* 2014; Planck Collaboration *et al.* 2015; Flores-Cacho *et al.* 2016). It is similarly important to stress that not all other spectroscopically-identified $z > 2$ proto-clusters have the sensitive submillimeter datasets needed to detect potential DSFG member galaxies (e.g. Lee *et al.* 2014).

3. FROM DSFG-RICH PROTO-CLUSTERS TO $Z \sim 0$ CLUSTERS

Such physically large, extended structures – like those observationally identified in § 2 – are not certain to collapse into massive galaxy clusters. How can we adequately determine whether or not these structures will collapse by $z \sim 0$? And does their number density agree with what is known about galaxy clusters at $z \sim 0$?

3.1. Will they collapse?

Two schools of thought have been used to address this question. The first draws on the Press-Schechter formalism (Press & Schechter 1974) for spherical collapse within large scale structure (Mo & White 1996), whereby a certain mass overdensity, δ_{mass} , is required to exceed a specific critical value δ_c to collapse by $z \sim 0$ (Pea-

cock 1999). Because the mass overdensity is not directly observable, linear galaxy bias is assumed whereby $1 + b\delta_{\text{mass}} = C(1 + \delta_{\text{gal}})$, and δ_{gal} is the observed galaxy overdensity, b is the bias associated with that galaxy population (i.e. how well they trace the dark matter halo mass), and C is a redshift distortion factor accounting for unknown peculiar velocities.

For example, the analysis of the GOODS-N $z = 1.99$ structure in Chapman *et al.* (2009) finds an SMG overdensity of $\delta = 10$, sufficient to cause collapse, however the underlying LBG population overdensity, $\delta_{\text{LBG}} = 2.5$, is not significant enough to cause collapse. These two assessments of the structure are seemingly contradictory, but the authors address this contradiction by suggesting that either the bias of the submillimeter galaxy population is sufficiently different than for LBGs, or there could be a large population of massive galaxies that have not been detected surrounding the structure. Given the depth of multiwavelength imaging in GOODS-N the latter is unlikely. Thus Chapman *et al.* determined that the bias for SMGs (or DSFGs) and LBGs was sufficiently different, and so even a large overdensity of SMGs may not probe massive clusters in formation.

This conclusion is further supported in Miller *et al.* (2015) who use large-volume semi-analytic simulations from Klypin, Trujillo-Gomez & Primack (2011) to argue that SMGs are “poor tracers” of the most massive structures at $z \sim 2$, observing very few massive structures containing more than 1–3 SMGs. The structures observed with >5 SMGs are indeed amongst the most massive, but are exceedingly rare in the simulation, much more so than the observations in § 2 suggest. This discrepancy between their predicted number of DSFG-rich proto-clusters and our observations are shown as green and blue points on the cluster mass function plot in Figure 1, discussed in more detail in the next subsection.

Note that other simulation groups (Granato *et al.* 2015; Lacey *et al.* 2015) have been working to understand the turn-on of luminous DSFGs in large-box simulations where the collapse of the most massive structures can be seen. The advantage of these techniques is the ability to directly constrain SMGs’ physical drivers, which they largely attribute to disk instabilities and a mildly top-heavy IMF. However, as highlighted in those works, it is still incredibly challenging to carry through proper radiative transfer in such large environments, especially on ~ 20 cMpc scales before clusters have collapsed.

The second school of thought draws on recent cosmological simulations of hierarchical growth, which produce somewhat different predictions than those relying on analytic descriptions of structure formation theory. For example, Chiang, Overzier & Gebhardt (2013) present a clear argument as to why spherical collapse models and the assumed linear regime for overdensities may introduce systematic errors in mass measurements for non- virialized proto-clusters. These direct predictions from simulations suggest that: (a) the median observed galaxy overdensity, δ_{gal} , rarely, if ever, exceeds 10 (this agrees with the predictions given in Miller *et al.* 2015), (b) δ_{gal} at these epochs also depends strongly on the observational characteristics being selected for, for example SFR or stellar mass, and sensibly vary between DSFG populations (very high SFR-selected samples) and LBG populations (a combination of SFR and mass selected, at

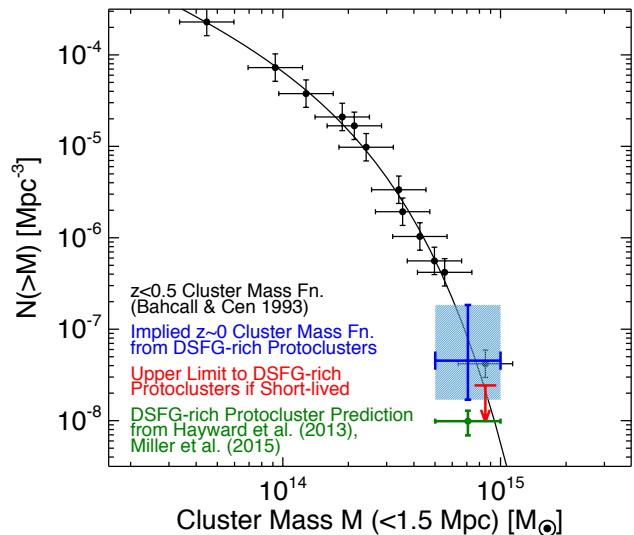


FIG. 1.— A comparison of the Cluster Mass Function from Bahcall & Cen (1993) against the extrapolated estimate of DSFG-rich proto-cluster descendants (blue point). The uncertainty is dominated by the limited understanding of the DSFG-rich proto-cluster selection function, and the survey area from which they have been found; future large-area surveys will enable a much more accurate constraint. If DSFG-rich proto-clusters are assumed to be a short-lived phenomenon, then an upper limit (red arrow) marks maximum density for DSFG-rich structures. The estimate of DSFG-rich proto-clusters (i.e. those with five or more DSFGs) from large-box *Bolshoi* simulations is shown as the green point (Hayward *et al.* 2013; Miller *et al.* 2015).

much deeper detection thresholds), (c) the progenitors of massive galaxy clusters at $z > 2$ occupy very large Lagrange volumes, $\gtrsim 10000$ cMpc³ (see also Oñorbe *et al.* 2014), and (d) δ_{gal} will vary for structures of the same mass depending on the ‘window size’ of observations, or presumed volume, given intrinsic variations in the underlying density along filaments.

For example, a close inspection of Figure 8 in Chiang, Overzier & Gebhardt (2013)— a plot of the cumulative fraction of proto-clusters with observed galaxy overdensities δ_g at $z = 2, 3, 4$ and 5 —provides a backdrop to interpret the likelihood of proto-cluster collapse. Among the five rich $1.99 < z < 3.09$ proto-clusters described in § 2, all structures are expected to collapse by $z \sim 0$. The structure with the least remarkable LBG overdensity at $\delta_{\text{gal}} = 2.5$, the GOODS-N $z = 1.99$ structure, is still among the top 30% of collapsing structures. The remainder are in the top 5–10%.

It should be clarified, however that the three highest redshift overdensities discussed in § 2 and summarized in Table 1 have a less clear fate. With far fewer numbers of galaxies (in both rare sub-types and total number), Poisson noise dominates the calculation of the overdensities, causing a wide margin of error on the structures’ predicted state at $z \sim 0$. These are the types of structures which may either be prone to mass overestimation, due to the effects discussed in Miller *et al.* (2015), or suffer from incomplete spectroscopic descriptions, though the latter interpretation may be limited by constraints set by the volume density of DSFG-rich proto-clusters as a whole.

3.2. How common are they?

While the argument for the eventual collapse of DSFG-rich proto-clusters into the most massive $z \sim 0$ clusters has been made in § 3, it is not immediately obvious that this evolutionary picture is feasible or likely, given the relatively small number of high-mass clusters at $z \sim 0$. In Figure 1, the cluster mass function at $z \lesssim 0.2$ is shown from the Sloan Digital Sky Survey (Bahcall & Cen 1993; Bahcall *et al.* 2003). This tells us that there is one $>10^{15} M_{\odot}$ cluster per every 1–2 million Mpc^3 , or per $\sim 120 \times 120 \times 120 \text{ Mpc}$ comoving box.

We can also work out a rough estimate to the volume density of DSFG-rich proto-clusters for comparison. A significant discrepancy between the volume density of $z \sim 0$ massive clusters and $z \gtrsim 2$ DSFG-rich proto-clusters is a sign that the two populations are not likely related¹. This was claimed to be the case in Blain *et al.* (2004), after analyzing the overdensity associated with the GOODS-N $z = 1.99$ structure, and a few other potential SMG-rich overdensities perceived in the first few square degrees of deep submm imaging. Blain *et al.* determined that DSFG-rich structures were unlikely to be the progenitors of massive clusters in formation because they are ~ 10 times more common at $z \gtrsim 2$ than their $z \sim 0$ descendants, which was reflective of the best data on-hand at the time. Here this estimation is reassessed with improved datasets.

To estimate the volume density of DSFG-rich proto-clusters at $z \gtrsim 2$, understanding survey area and selection bias is critical. Survey area in this case is set by the solid angle of sky covered to sufficient depth to recover DSFG-rich structures at high-redshift. This requires both spectroscopically complete samples *and* confusion-limited submillimeter blank-field maps. Both are extremely limited by current observational resources. The former is limited by the need for several tens of nights on 8–10 m class optical/near-infrared telescopes for multi-object spectroscopy of faint $i \sim 22 - 26$ sources (of which only a few fields have truly complete coverage, e.g. GOODS-N, central portion of COSMOS, ECDF-S), and the later is limited by the historically slow mapping speeds of single-dish bolometer array instruments like SCUBA (also LABOCA, MAMBO, AzTEC, and now SCUBA-2). The intersection of these two datasets is therefore limited to:

- about 0.4 deg^2 in GOODS-N, a field with confusion limited $850\mu\text{m}$ data (Barger *et al.* 1998; Chen *et al.* 2013) and extensive spectroscopic completeness (Cowie *et al.* 2004; Wirth *et al.* 2004; Reddy *et al.* 2006; Barger, Cowie & Wang 2008),
- the central 1 deg^2 of the COSMOS field, which has published confusion-limited $850\mu\text{m}$ data covering 0.2 deg^2 (more yet in Geach *et al.*, in prep), and 1 deg^2 of deep spectroscopic data from the zCOSMOS team (Lilly *et al.* 2009),
- about 0.5 deg^2 in ECDF-S with confusion-limited submm data from LABOCA and ALMA (Wei *et al.* 2009; Hodge *et al.* 2013) and spectroscopic

follow-up from Popesso *et al.* (2009), Balestra *et al.* (2010), and Le Fvre *et al.* (2005), and

- a 0.5 deg^2 portion of the Lockman Hole (SHADES) field with for which a significant number of DSFGs have been spectroscopically confirmed (Chapman *et al.* 2005; Lindner *et al.* 2011; Casey *et al.* 2012), and
- other deep submillimeter fields, which include the backgrounds of low-redshift Abell clusters (e.g. Smail, Ivison & Blain 1997; Chen *et al.* 2013) and the SSA13 and SSA22 fields, and cumulatively add up to about $\sim 0.5 \text{ deg}^2$.

This collection of deep surveys adds up to a total effective survey solid angle of $\sim 3 \text{ deg}^2$, with an uncertainty of about $\sim 0.5 \text{ deg}^2$ to account for variable levels of spectroscopic completeness and submm data quality and depth. While it should be noted that *Herschel* coverage also spans all of these legacy fields, the intersection with spectroscopic samples is the main limiting factor in making use of it for this analysis. In addition, *Herschel* is most efficient at identifying DSFGs at $z < 2$ (Casey *et al.* 2012), a characteristic of its shorter-wavelength selection than ground-based submm datasets. Color selection with the *Herschel* bands seems like an efficient method of recovering a higher-redshift sample (e.g. Dowell *et al.* 2014; Asboth *et al.* 2016), though the depth and completeness of these ‘ $500\mu\text{m}$ -peakers’ is less well characterized. It is important to emphasize that this estimation is very rough, as the complexity of these datasets is incredibly difficult to quantify in a simple analysis.

The corresponding solid angle to this 3 deg^2 is converted to a cosmological comoving volume within the redshift interval of interest, which is approximated as $1.9 < z < 4.5$, the lower limit defined by the limit of known virialized clusters and the upper limit constrained by low completeness in most large spectroscopic surveys summarized above. Allowing for some additional uncertainty in the redshift interval, the total volume accessible is $(9 \pm 3) \times 10^7 \text{ cMpc}^3$. By chance this is approximately the same volume probed by deep SDSS cluster surveys, $\sim 400 \text{ deg}^2$ out to $z \sim 0.1 - 0.2$ (Bahcall *et al.* 2003), from which the nearby cluster mass function is measured.

Though there are clearly these five, bona-fide DSFG-rich proto-clusters identified in the literature, one is substantially impacted by a possible selection bias associated with the proto-cluster. Much of the deep data associated with MRC1138–256 at $z = 2.16$ was obtained with the explicit knowledge of the proto-clusters’ presence, and so it cannot be included in the calculation estimating their volume density. Thus four DSFG-rich proto-clusters are left for the volume density calculation: GOODS-N at $z = 1.99$, COSMOS at $z = 2.10$, COSMOS at $z = 2.47$, and SSA22 at $z = 3.09$. A Poisson uncertainty is assumed for the number of DSFG-rich proto-clusters. The implied volume density is then $\sim 5 \times 10^{-8} \text{ cMpc}^{-3}$ for DSFG-rich proto-clusters. This is depicted by the blue point on Figure 1 and is in rough agreement with the observed $z \sim 0$ cluster mass function.

There is one remaining concern with this calculation. If this estimate is consistent with the $z \sim 0$ local cluster mass function, then it may imply *every* $z \gtrsim 2$ proto-cluster should be DSFG-rich. This is not obviously the

¹ Either they are not likely related, or if they are DSFG-rich proto-clusters are probably much more rare than most ‘normal’ proto-clusters.

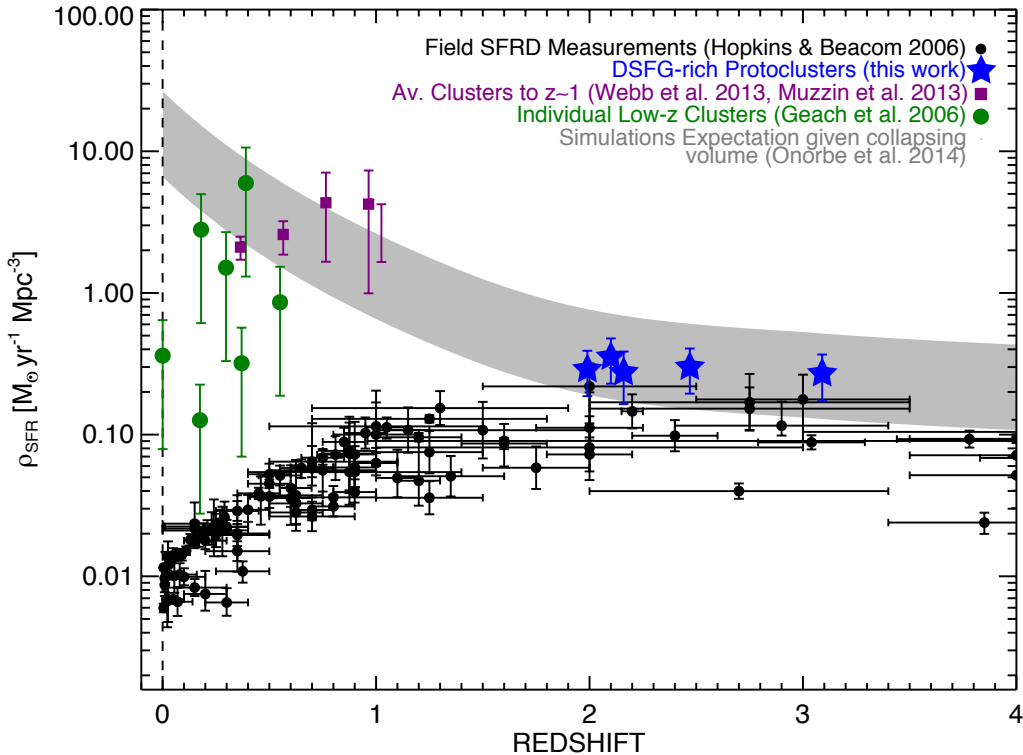


FIG. 2.— The star-formation rate density (ρ_{SFR} , in $M_{\odot} \text{ yr}^{-1} \text{ Mpc}^{-3}$) of proto-clusters and clusters, in comparison to galaxies in the field from Hopkins & Beacom (2006) (black points). The five DSFG-rich proto-clusters from this work are shown as blue stars, seven individual low-redshift clusters from Geach *et al.* (2006) are shown as green circles, and redshift-averaged results from 42 clusters at $0.3 < z < 1.0$ in Webb *et al.* (2013) shown in purple. The virialized clusters have an $\sim 2 \text{ Mpc}$ proper radius, and the associated volume is converted into comoving units for fair comparison with the field and proto-clusters. The gray stripe represents the track of a hypothetical and idealized proto-cluster which sustains a constant $\text{SFR} \approx 3000 \pm 1500 M_{\odot} \text{ yr}^{-1}$ from $z \sim 4$ to $z = 0$, but whose SFR density increases by a factor of ~ 100 from $z = 2$ to $z = 0$ due to the dramatic reduction in comoving volume as the cluster collapses and virializes. Real clusters may see this steep rise in ρ_{SFR} from $z = 2$ to $z = 1$, but then experience some type of quenching which cuts off ongoing star-formation at more recent times $z < 1$, as demonstrated by some of the low- z clusters shown in green and purple here.

case. Before addressing this issue further, one must first consider the timescale of DSFGs and their implications on clusters' assembly histories.

3.3. Star-Formation in DSFG-rich Proto-clusters

Placing DSFG-rich proto-clusters in context requires a more detailed look at their observable star-formation characteristics in comparison to the field (i.e. normal density regions), and lower redshift virialized clusters. Figure 2 shows the cosmic star-formation rate density from $0 < z < 4$ as compiled by Hopkins & Beacom (2006) for the field, against similar measures for overdense environments.

DSFG-rich proto-clusters at $2 < z < 3$ only have slightly elevated ρ_{SFR} than the field, thanks primarily to the large volumes they occupy prior to virialization. On the other hand, virialized clusters at $z < 1$ have substantially higher ρ_{SFR} , peaking around $0.5 < z < 1.0$, while potentially experiencing suppressed star-formation at lower redshifts brought on by different environmental mechanisms. Note that the comparison between virialized clusters and the field uses comoving volume, as opposed to proper volume, for fair comparison with structures which have not yet collapsed and decoupled from the Hubble flow. All values of SFR are converted to a Chabrier IMF (Chabrier 2003). The gray band marks the evolution of a hypothetical cluster that sustains an ag-

gregate SFR of $3000 M_{\odot} \text{ yr}^{-1}$ from $z = 4$ to $z = 0$ while undergoing collapse as predicted from large N-body simulations (Oñorbe *et al.* 2014). This highlights, through one variable, how galaxies in proto-clusters more closely emulate galaxies in the field than those in $z \sim 1$ clusters that have collapsed.

Figure 3 takes a closer look at the breakdown of the star-formation rate function, or luminosity function within a DSFG-rich proto-cluster in comparison to the field. For context, the Lyman-Break Galaxy luminosity function of Reddy & Steidel (2009) is converted to a SFR function using the UV-scaling in Kennicutt (1998) and applying a factor of five correction for extinction (i.e. most LBGs are 80% obscured; Reddy *et al.* 2012). The highest redshift luminosity function from the infrared (Gruppioni *et al.* 2013) is converted to a SFR also using the Kennicutt prescription, adjusted for a Chabrier IMF. Against these field measurements, the SFR function of DSFG-rich proto-clusters is shown: all of the known members of the COSMOS $z = 2.47$ proto-cluster (Casey *et al.* 2015) in red, and the DSFG member galaxies of all five $1.99 < z < 3.09$ structures in black stars. The key distinguishing characteristic of DSFG-rich proto-clusters is the flattening of the luminosity function towards high SFRs. While there may be an excess of LBGs observed in high- z proto-clusters, the excess is not as great as the factor $\gtrsim 10$ excess towards the highest SFRs.

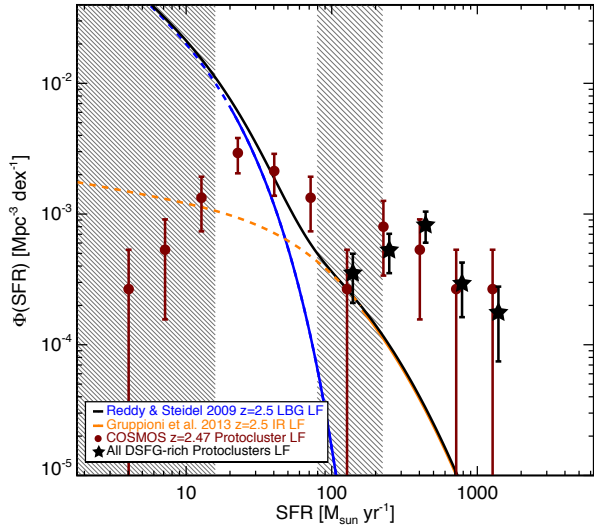


FIG. 3.— The star-formation rate function of DSGF-rich proto-clusters compared to the field. The luminosity functions of Lyman-break galaxies (blue line; Reddy & Steidel 2009) and IR-selected galaxies (orange line; Gruppioni *et al.* 2013) in the field are shown for context; the black line sums the two. The SFR function of the COSMOS $z = 2.47$ proto-cluster (red points) is shown for all known members. No correction has been made for incompleteness (hashed gray regions and dashed lines), which dominates at SFRs $\lesssim 20 M_{\odot} \text{yr}^{-1}$ (for UV-selected samples) and at $\text{SFR} \approx 100\text{--}200 M_{\odot} \text{yr}^{-1}$ (for DSGFs). The net SFR function for all five DSGF-rich proto-clusters at $1.99 < z < 3.09$ is shown as black stars.

4. SIMULTANEOUS TRIGGERING, OR NOT?

Here the likelihood of several rare types of galaxies being observed simultaneously within a large structure is explored. If you work from the premise that both populations of DSGFs and AGN are short-lived on 100 Myr timescales, then one can ask what the probability is of observing N of them simultaneously in one structure (where $N \gtrsim 5$). If the probability is low, and yet the prevalence of such DSGF-rich structures is high, then one may think this is evidence that clusters themselves assemble in rapid bursts, even when extended over very large volumes $\gtrsim 10000 c\text{Mpc}^3$ (as suggested in Casey *et al.* 2015).

Care should be taken in correcting for the dynamical time of each DSGF at different redshifts, as discussed in Simpson *et al.* (2014). At higher redshifts, a fixed dz element probes shorter and shorter timescales, such that the probability of observing *all* DSGFs which have been triggered during that time element dz increases from low fractions at low- z to 100% at high- z . While large redshift bins with widths $\Delta z = 0.1 - 0.2$ will probe all such episodes, it is important to note that the redshift range probed by a single coherent structure, $dz \approx 0.02$, only corresponds to a crossing time of ≈ 20 Myr, shorter than the expected duration of the burst phase. If this itself were to exceed the estimated lifetimes of our rare galaxies, that could provide an easy explanation as to why we observe structures that are quite rich in DSGFs and luminous AGN. However, that is not the case.

Another possible explanation for the plethora of rare galaxies is that we actually expect nearly all $z \sim 0$ galaxy cluster members to have gone through such a rare phase at some time in its past, probably around $z \sim 2 - 3$. But

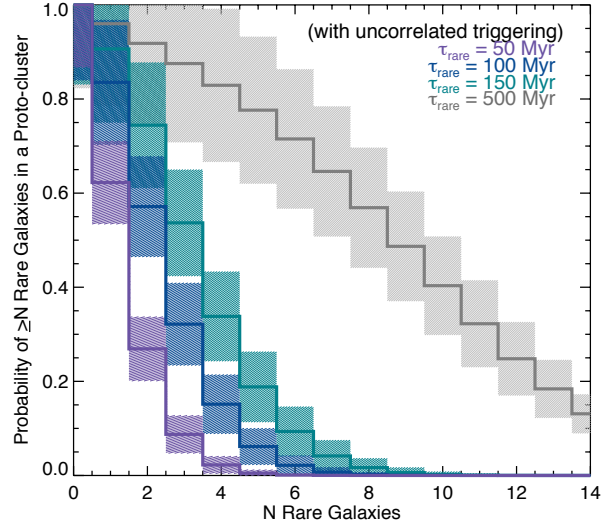


FIG. 4.— The probability of observing $\geq N$ rare galaxies (including DSGFs and luminous AGN) simultaneously in one proto-cluster structure, if uncorrelated, random triggering is assumed. With 40 ± 10 massive $> 10^{11} M_{\odot}$ galaxies in present-day massive galaxy clusters (van der Burg *et al.* 2013), one can assume all of them passed through a DSGF phase at some point between $1 < z < 6$ in which they build the majority of their mass. If the rare galaxies are triggered at random during that time/redshift interval (i.e. they are uncorrelated events) the likelihood that N or more of them would be ‘on’ simultaneously is shown, given an average lifetime of 50 Myr (purple), 100 Myr (blue), 150 Myr (teal), or 500 Myr (gray). For example, if DSGFs are short-lived, the likelihood of observing > 3 per structure is very low. Conversely, if DSGFs are long-lived, we are more likely to see structures with ≥ 8 DSGFs than with fewer.

in investigating this further, there is a problem. The most massive galaxy clusters at $z \sim 1$ only have 40 ± 10 galaxies above a stellar mass of $10^{11} M_{\odot}$ (van der Burg *et al.* 2013). If one presumes all of these have gone through a DSGF phase at some point during their mass buildup (as most of them are quiescent by $z = 0.5 - 1$), then by working backwards, the likelihood of observing N of them in a DSGF or luminous AGN phase simultaneously can be worked out. Here the time T it takes for the structure to collapse from its primordial fluctuations is relatively unknown, but is loosely constrained by the redshift interval $1 < z < 6$ (≈ 5 Gyr), or $2 < z < 5$ (≈ 2 Gyr).

Figure 4 shows the probability of simultaneously observing $\geq N$ DSGFs/AGN within one structure forming over the course of 2 Gyr. Assuming a 2 Gyr timescale renders the probability calculations in Figure 4 conservative, as allowing for longer fall-in times makes the probabilities of observing multiple DSGFs simultaneously only lower. Four different rare-galaxy timescales are assumed (where ‘rare’ can refer to either the DSGFs or the short-lived, luminous AGN in this case): 50 Myr (in line with what is observed in local ULIRGs; Solomon & Sage 1988), 100 Myr (the typical DSGF timescale and upper limit to QSO lifetimes; Greve *et al.* 2005; Martini 2004), 150 Myr (a depletion time typical of some longer lived DSGFs at high-redshift; Swinbank *et al.* 2014), and 500 Myr (a DSGF timescale which would rely on some sustained gas fueling, which some assert is likely the case at the massive end of the galaxy ‘main-sequence;’ Elbaz *et al.* 2011). This figure illustrates that the assumed timescale for DSGFs and luminous AGN is rather important to our

understanding of cluster assembly. Over a 2 Gyr build time, if DSFGs/AGN are short-lived then the probability of observing >5 such sources in one proto-cluster structure is $<0.5\%$ (50 Myr), 6.1% (100 Myr), 19% (150 Myr), 77% (500 Myr). However, structures like the COSMOS $z = 2.47$ structure and SSA22 contain 12 rare sources *each*.

With a short-lived phase, this is virtually impossible through uncorrelated triggering ($<1 \times 10^{-4}\%$), and still yet unlikely for long duration events ($<25\%$). If such phenomena are short-lived, then they most certainly are triggered simultaneously in an event that stretches across very large volumes. One can imagine this triggering is brought on by the rapid collapse of filamentary structure that extends across several tens of Mpc.

On the other hand, the test above seems to suggest that longer lifetimes are far more likely (by over a factor of ten) for DSFGs and luminous AGN in proto-clusters. Recent simulations work (Narayanan *et al.* 2015) suggest that even somewhat isolated DSFGs could sustain sufficiently high star-formation rates ($\gtrsim 500 M_{\odot} \text{ yr}^{-1}$) for 0.75 Gyr. Physically, this sounds plausible particularly in dense environments, where high star-formation rates may be sustained over longer periods of time if the galaxies are continually fed fresh supplies of gas from the surrounding, rich medium. In the next few subsections, I explore observations which support both rapid collapse and heightened gas supply scenarios.

4.1. Molecular Gas Depletion Time

Determining the correct interpretation of the assembly history of galaxy clusters requires direct constraints of the molecular gas potential wells in proto-cluster DSFGs. This gives critical information on galaxies' current gas supply, and over what time period such high star-formation rates would be continuously sustainable. To reiterate, this is a particularly useful measurement in DSFGs due to their rarity, as demonstrated in the previous section.

Table 5 summarizes existing CO observations of proto-cluster DSFGs from the literature. Though limited in number and heterogeneous in transition and depth, these data can begin to discern the plausibility of short-lived versus long-lived interpretations. However, as with most previous work on high- z CO observations it is very important to recognize that the conversion from observed CO line strength to H_2 gas mass is highly uncertain. It first requires a conversion from a high-J CO transition to the ground state CO(1-0), which requires knowledge of the galaxy's mean CO excitation ladder, or kinetic gas temperature. Second, the conversion from CO(1-0) to M_{H_2} , known as X_{CO} or α_{CO} , can also range by factors of 5–10 depending on gas conditions in the ISM. For example, the Milky Way has a gas conversion rate of $\alpha_{CO} = 4.5 M_{\odot} (\text{K km s}^{-1} \text{ pc}^2)^{-1}$ (Bloemen *et al.* 1986; Solomon *et al.* 1987) while typical local ULIRGs have $\alpha_{CO} = 0.8 M_{\odot} (\text{K km s}^{-1} \text{ pc}^2)^{-1}$ (Downes & Solomon 1998). The uncertainties in these two conversions alone can account for a factor of $\gtrsim 10$ in the predicted gas mass, which could dramatically affect the interpretation of the depletion timescale, $\tau_{\text{depl}} = M_{H_2}/\text{SFR}$.

For those proto-cluster DSFGs without CO(1-

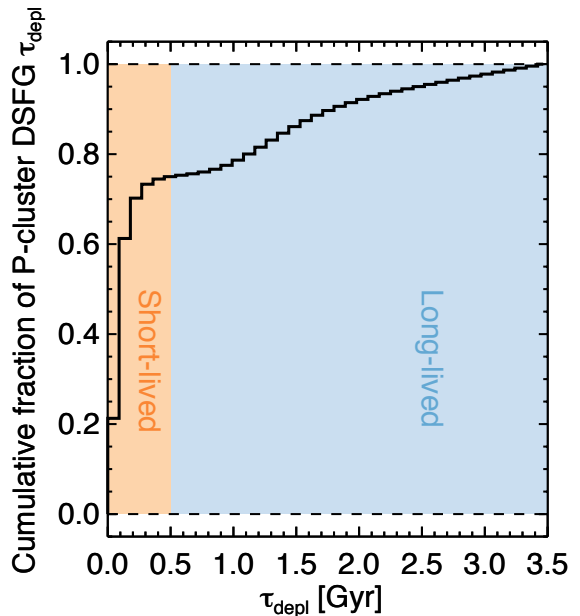


FIG. 5.— The cumulative distribution of gas depletion times for DSFGs in proto-clusters as given in Table 5. Each of the eight source's depletion times is represented as a Gaussian with associated uncertainty. Here $\tau_{\text{depl}} = M_{H_2}/\text{SFR}$, and M_{H_2} is estimated from observations of CO. While only eight proto-cluster DSFGs in the literature have CO measurements, the majority are consistent with short depletion times, $\lesssim 200$ Myr (60%), supporting the idea that proto-clusters endure wide-scale star-forming bursts.

0) observations, a CO gas excitation ladder, and associated uncertainties, is assumed as given in Bothwell *et al.* (2013), the median excitation seen in all observed DSFGs to-date. Their figure 3 shows this median DSFG spectral line-energy distribution. Each high-J CO line luminosity in Table 5 is thus converted to an estimated CO(1-0) line luminosity via $L'_{CO(1-0)}/L'_{CO(J-[J-1])} = (S_{CO(1-0)}/S_{CO(J-[J-1])})(1/J)^2$. The uncertainty in the CO Spectral Line Energy Distribution (SLED) is reflected in the resulting uncertainty of CO(1-0) line luminosity. The conversion from $L'_{CO(1-0)}$ to M_{H_2} assumes $\alpha_{CO} = 1.0 M_{H_2} (\text{K km s}^{-1} \text{ pc}^2)^{-1}$, the same value adopted in Bothwell *et al.* (2013) and justified generally through some limited dynamical mass constraints. The resulting gas masses M_{H_2} are given in Table 5, with some proto-cluster DSFGs containing multiple components. In the case where multiple high-J CO transitions are observed for a single galaxy, a molecular gas mass is derived for each independently, then averaged. Depletion times are then calculated by taking the total molecular gas mass estimated to be present in the system and dividing by the current star-formation rate, as calculated in § 2. The probability distribution in depletion times is shown in Figure 5. Though quite sparse, the majority of sources ($5/7 \approx 71\%$) are estimated to be short-lived, with $\tau_{\text{depl}} \lesssim 150$ Myr.

4.2. Evidence supporting rapid bursts in Proto-clusters

The discussion presented on the measured molecular gas depletion time of DSFGs in proto-clusters heavily favors a rapid collapse model, whereby the massive galaxies in clusters are built in short-lived, extreme episodes that permeate the entire volume of the not-yet-virialized proto-

TABLE 5
DSFGs IN PROTO-CLUSTERS WITH CO MEASUREMENTS

DSFG Name	z	Transition	L'_{CO} [K km s ⁻¹ pc ²]	$M(\text{H}_2)^\diamond$ [M_\odot]	SFR [$M_\odot \text{ yr}^{-1}$]	τ_{depl} [Myr]	Reference
DETECTIONS:							
DSFG J123618+621550	1.996	CO(4-3)	$(9.4 \pm 1.4) \times 10^{10}$	$(2.6 \pm 0.6) \times 10^{11}$			Bothwell <i>et al.</i> (2010)
	2.001	CO(4-3)	$(6.5 \pm 0.9) \times 10^{10}$	$(1.8 \pm 0.4) \times 10^{11}$			Bothwell <i>et al.</i> (2010)
			<i>total:</i>	$(4.4 \pm 0.7) \times 10^{11}$	330_{-80}^{+110}	1300 ± 400	
DSFG J123711+621331	1.988	CO(4-3)	$(1.3 \pm 0.2) \times 10^{10}$	$(3.6 \pm 0.8) \times 10^{10}$			Casey <i>et al.</i> (2011)
	1.996	CO(4-3)	$(7.8 \pm 1.1) \times 10^9$	$(2.2 \pm 0.5) \times 10^{10}$			Casey <i>et al.</i> (2011)
	1.995	CO(3-2)	$(1.5 \pm 0.5) \times 10^{10}$	$(3.4 \pm 1.2) \times 10^{10}$			Casey <i>et al.</i> (2011)
			<i>average:</i>	$(4.9 \pm 0.7) \times 10^{10}$	540_{-210}^{+350}	110 ± 60	
DSFG J123712+621322	1.996	CO(4-3)	$(6.8 \pm 1.5) \times 10^9$	$(1.9 \pm 0.5) \times 10^{10}$			Casey <i>et al.</i> (2011)
	1.996	CO(3-2)	$(2.7 \pm 0.9) \times 10^{10}$	$(6.0 \pm 2.2) \times 10^{10}$			Bothwell <i>et al.</i> (2013)
			<i>average:</i>	$(2.1 \pm 0.5) \times 10^{10}$	190_{-90}^{+170}	110 ± 80	
DSFG J123632+620800	1.994	CO(3-2)	$\ddagger(4.0 \pm 1.1) \times 10^{10}$	$(8.9 \pm 2.8) \times 10^{10}$	36_{-30}^{+144}	$\lesssim 9000$	Bothwell <i>et al.</i> (2013)
DSFG J114048–262908	2.163	CO(1-0)	$(6.5 \pm 0.6) \times 10^{10}$	$(6.5 \pm 0.6) \times 10^{10}$			Emonts <i>et al.</i> (2013)
	2.150	CO(1-0)	$(6.9 \pm 2.3) \times 10^9$	$(6.9 \pm 2.3) \times 10^9$			Emonts <i>et al.</i> (2013)
					$\ddagger 740 \pm 80$	97 ± 13	Seymour <i>et al.</i> (2012)
DSFG J114046–262913	2.147	CO(1-0)	$(3.3 \pm 0.2) \times 10^{10}$	$(3.3 \pm 0.2) \times 10^{10}$	$\ddagger 480_{-110}^{+150}$	68 ± 5	Emonts <i>et al.</i> (2013)
DSFG J221735+001537	3.096	CO(3-2)	$(3.8 \pm 1.0) \times 10^{10}$	$(8.5 \pm 2.5) \times 10^{10}$	$\heartsuit 1100_{-200}^{+300}$	80 ± 30	Greve <i>et al.</i> (2005)
DSFG J221726+001239	3.102	CO(4-3)	$(6.7 \pm 2.1) \times 10^{10}$	$(1.9 \pm 0.7) \times 10^{11}$	140_{-600}^{+1100}	140 ± 90	Chapman <i>et al.</i> (2004)
DSFG J221732+001744	3.092	CO(3-2)	$\flat 1180_{-230}^{+890}$...	(Yun <i>et al.</i> , in prep)
NON-DETECTIONS:							
DSFG J123621+621708	1.973–2.008	CO(4-3)	$< 5.2 \times 10^9$	$< 1.5 \times 10^{10}$	310_{-110}^{+170}	< 50	Bothwell <i>et al.</i> (2013)
DSFG J123600+621047 [‡]	1.971–2.017	CO(3-2)	$< 2.9 \times 10^{10}$	$< 6.5 \times 10^{10}$			Greve <i>et al.</i> (2005)
		CO(3-2)	$< 1.6 \times 10^{10}$	$< 3.6 \times 10^{10}$			Bothwell <i>et al.</i> (2013)
					110_{-50}^{+100}	< 300	

Table Notes.

[◇] Gas masses estimated assuming a fixed α_{CO} gas conversion factor of $\alpha = 1.0$ (as in Bothwell *et al.* 2013).

[†] tentative detection of CO.

[‡] SFR for the Spiderweb galaxy is calculated from the starburst component of the FIR SED as presented in Seymour *et al.* (2012).

[‡] SFR for HAE source at $z = 2.147$ is taken from H α measurements from Kurk *et al.* (2004) as 23 ± 1 ; however, we refit the SFR given the FIR photometry measured in Dannerbauer *et al.* (2014) (their table 4).

[♥] SFR for the SSA22 galaxy calculated from 850 μm flux density and radio flux density using an SED with temperature 35K from Chapman *et al.* (2005), also accounting for a deboosting factor ~ 1.5 , consistent with more recent submm datasets.

[♭] SFR calculated as in Umehata *et al.* (2015).

[‡] SMG-93, a.k.a. SMM J123600+621047 is mistakenly labeled as SMM J123600+620253 in Bothwell *et al.* (2013), but all of the physical characteristics listed in Bothwell *et al.* are indeed for SMG-93.

cluster. The measured gas depletion times for proto-cluster DSFGs (as presented in Table 5 and Figure 5) are the most crucial constraint to this argument, but it is significantly strengthened by inferred constraints on the lifetimes of AGN with comparable luminosities to unobscured quasars (Marconi *et al.* 2004). The strong evidence for short-lifetimes, combined with the low probability of observing $N \gtrsim 5$ of these rare galaxies in one structure, argue for correlated, simultaneous triggering. Such simultaneous triggering has been directly demonstrated in smaller isolated cases, as in Ivison *et al.* (2013), though not on physical scales this large. If correct, the result is rather extraordinary, as it represents the only type of direct observation of a temporal ‘event’ on cosmological scales, spanning a volume $\sim 10^4 \text{ cMpc}^3$. In the next subsection, I briefly explore evidence which supports the contrary conclusion.

4.3. *Evidence in favor of Gradually-Built Proto-clusters*

Though analysis of literature DSFGs in proto-clusters suggests they are mostly short-lived, the impact of our high-J CO to gas mass assumptions should be revis-

ited. If our assumptions were to be revised in favor of more ‘Milky Way’ type gas excitation and higher intrinsic value of α_{CO} , the CO(1-0) line luminosities would be a factor of ~ 3 higher, and the gas masses a factor of ~ 20 higher. The median depletion time of 110 Myr would instead be 2.2 Gyr, much more in line with the predicted long-lifetimes of DSFGs in some cosmological simulations (Narayanan *et al.* 2015). Reducing the intrinsic uncertainty in this measurement requires CO(1-0) measurements of a larger sample of proto-cluster DSFGs with additional resolved dynamical mass constraints to hone in on the correctly applicable α_{CO} . Some of these observations are currently underway at the Jansky Very Large Array. However, it should be noted that there is a known upper limit to how long DSFGs can sustain high-SFRs, given by stellar mass constraints for the Universe’s most massive galaxies. For example, a galaxy cannot reasonably maintain a $500 M_\odot \text{ yr}^{-1}$ star-formation rate for longer than 1 Gyr or so, else the mass of stars produced will exceed $5 \times 10^{11} M_\odot$.

Another possible caveat to our rapid collapse argument is the possibly heightened replenishment of gas

reservoirs from the IGM. It has recently become clear that galaxies recycle gas through ejective feedback and outflows, and the eventual reaccretion of material on \sim Gyr timescales (Christensen *et al.* 2015); however, it is unclear how dense environments at the intersections of filaments in the IGM might shorten the gas recycling timescale and potential heightened inflow of pristine material. If molecular gas is fed onto galaxies more efficiently in proto-clusters than in the field, particularly on \sim 100 Myr timescales, then the depletion time measurement might not be an accurate reflection of the lifetime of high-SFR systems. However, such a dramatically fast (\lesssim 100 Myr) replenishment of $\sim 10^{10} M_{\odot}$ gas reservoir is unlikely, again due to the upper limit placed on high-SFR timescale from observed stellar mass functions.

Finally, as mentioned at the end of § 3.2, the frequency of DSFG-rich proto-clusters among the population of all proto-clusters raises a potential concern. If the timescale of the DSFG-rich phase is short-lived and unique, then one may only expect a small subset of observed $z > 2$ proto-clusters to have such DSFG excesses. To gauge the plausibility of this argument, we should consider how many member galaxies we *expect* to go through such a phase over the course of a cluster’s lifetime. In § 4, this was approximated as 40 ± 10 massive $> 10^{11} M_{\odot}$ galaxies. If there are 5–10 rare galaxies per proto-cluster, then we may expect such structures to go through 4–8 “episodes” of heightened activity before virialization at $z < 2$. If these episodes are assumed to all occur between $2 < z < 5$ (≈ 2 Gyr) then one would expect ~ 20 – 40% of all proto-clusters of that epoch to be DSFG-rich assuming a 100 Myr ‘burst’ lifetime. With a 150 Myr lifetime, the fraction shifts to ~ 30 – 60% , and at 50 Myr only ~ 10 – 20% . Though these fractions are certainly non-negligible, it is clear that it would be nearly impossible for *all* $z > 2$ proto-clusters to be DSFG-rich *if* they are short-lived and therefore our comparison to the measured cluster mass function at $z \sim 0$ might disfavor short timescales. It is certainly clear that refining measurements of the volume density of high- z proto-clusters is needed before ruling out different histories of their assembly.

5. PREDICTIONS

5.1. Future Observations

The most important observational characteristic of massive galaxy clusters is the large area they subtend on the sky, \sim half a degree across. While some recent works have recognized the importance of this (e.g. Muldrew, Hatch & Cooke 2015), the observational community which works on proto-cluster science has largely overlooked the shear scale of early, overdense structures. It is critical to address this if we desire to move beyond simple proto-cluster discoveries and learn about the collapse of large scale structure from an observational perspective.

The next generation of wide field (and sufficiently deep) surveys – on order tens of square degrees – will be of great importance to identifying statistically large samples (~ 100) of proto-clusters, both those with and without rare galaxies. The most efficient means of confirming high-redshift overdensities like these will be through direct far-infrared/millimeter molecular line detection, which may only be efficient on large scales with the next

generation of submm single-dish multi-pixel spectrometers. The relative fraction of such structures with rare galaxies will, in turn, allow the more detailed look at all clusters’ temporal evolution.

On slightly smaller angular scales, recent work from Clements *et al.* (2014), Planck Collaboration *et al.* (2015) and Flores-Cacho *et al.* (2016) search out proto-clusters rich in dusty star-formation by leveraging the poor spatial resolution of the *Planck* satellite, which covers the entire sky. Following-up *Planck*’s $\sim 5'$ point sources with the higher resolution *Herschel Space Observatory* is hoped to be an efficient way of identifying early clusters in formation. While none have yet been spectroscopically confirmed, over 200 candidate high-redshift clusters have been identified with an excess of dusty starbursts peaking at $\gtrsim 350 \mu\text{m}$. The technique is certainly promising though will be quite incomplete in the type of structure discussed in this paper, as many dusty starbursts would need to fall in one *Planck* beam, much smaller than the previously discussed half-degree scale.

In terms of characterizing known structures more fully, narrow-band imaging should provide the most complete mapping of filamentary structures on the largest scales. This is the case in the SSA22 $z = 3.09$ structure, as well as some structures not observed in the submillimeter (e.g. the Boötes $z = 3.78$ structure; Lee *et al.* 2014) but has not been pursued over sufficiently large angular scales for most proto-clusters. Similarly, wide-field IFU spectroscopic follow-up will be quite valuable, from facilities like the VIRUS instrument on the Hobby-Eberly Telescope.

It is clear that understanding galaxies’ gas supply is an essential element in discerning proto-clusters’ assembly history, and in the age of ALMA and the Jansky VLA, is not limited to the most luminous, rare galaxies. Scaling of long-wavelength dust continuum to an ISM mass has shown to be a useful proxy (Scoville *et al.* 2014, 2015) to galaxies’ star-forming molecular gas masses. Thus fairly inexpensive observational campaigns to constrain the gas content of proto-clusters’ normal galaxy members might provide more important clues as to how environment influences galaxies’ evolution.

5.2. Simulations

Simulations of large-scale structure collapse on cosmological scales plays a crucial role in our current picture of galaxy cluster formation, linking the huge gap between observations of nearby virialized clusters and the imprint of density perturbations on the Cosmic Microwave Background. Large-box > 100 Mpc simulations are certainly needed to analyze $> 10^{15} M_{\odot}$ halos. Their enormous volumes limit the incorporation of baryonic physics and force the implementation of ultraluminous starbursts, or luminous AGN, to be somewhat crude. Yet, there are some basic measurements which could be extracted from the current generation of simulations that would shed ample light on the proposed assembly history of massive galaxy clusters. In dark-matter only simulations, the most direct probe of cluster assembly is the merging of dark matter halos with time. These merger trees, mapped with spatial distribution, could directly trace whether or not growth of halos, and thus the galaxies living in them, is episodic or steady.

Beyond the measurement of stochasticity in assembly,

simulations will be needed to more accurately constrain dark matter halo masses from observations. While it is clear that linear bias assumptions break down under certain pretexts, it is not entirely appropriate to use normal abundance matching techniques which are more ideally suited for isolated halos. An in-depth look at halo mass distributions in proto-clusters before virialization might provide crucial insight that bridges our theoretical understanding to observational constraints.

6. CONCLUSIONS

This paper has employed literature datasets to demonstrate that several high-redshift proto-cluster environments are rich with rare galaxies: both dusty star-forming galaxies and ultraluminous AGN. These proto-clusters subtend $10'$ to a half degree in the sky because they have not yet relaxed into virialized galaxy clusters. By virtue of their large occupied volumes at $z \gtrsim 2$ (factors of a few hundred larger than at $z \sim 0$), it is very difficult to detect their significance via an overdensity of ‘normal’ galaxies on appropriately large scales, which are only slightly more dense than the field. Instead, an unexpected excess of rare galaxies ($\gtrsim 5$ per $\sim 10^4$ cMpc³ volume) can demonstrate a more compelling argument for a large-scale proto-cluster in formation.

Five bona-fide DSFG-rich proto-clusters have been identified to-date within $1.99 < z < 3.09$. Estimates to their volume density—constrained by deep spectroscopic and submm datasets—is $\sim 5 \times 10^{-8}$ cMpc⁻³, similar to the density of observed $> 10^{15}$ M_⊙ clusters at $z < 0.2$. Some simulations work expect the volume density of DSFG-rich structures to be a factor of ~ 5 less than observed.

The rarity of DSFGs and luminous AGN relates to their intrinsically short duty cycle. If this population is predominantly short-lived, then it can be used as a constraint on the assembly history of galaxy clusters in the time before virialization. For example, the probability of observing 10 or more 100 Myr-duration rare galaxies in one structure is $< 0.01\%$. This suggests the phenomenon is exceedingly rare, and yet there are several multiple DSFG-rich proto-clusters in only a few square degrees of data. The existence of these structures provides direct observational evidence that proto-clusters assemble in short-lived, stochastic bursts that likely correspond to

the collapse of large-scale filaments on 10 Mpc scales. In this sense, such episodes represent “events” observed on the largest scales seen since the imprint of recombination from the CMB.

An alternate view may be that the gas potential wells of DSFGs in proto-clusters are much deeper, fueled by an excess of gas in the surrounding IGM. This point of view would argue for more long-lived DSFGs. If this is the case, then it is more likely that DSFGs in proto-clusters are triggered at somewhat arbitrary times determined only by their local < 1 Mpc surrounds. As a result, it is also likely that nearly every observed proto-cluster is DSFG-rich. The evidence that supports this claim is our estimate of the volume density to DSFG-rich proto-clusters and its agreement with the cluster mass function. If such DSFGs are short-lived, then at most \sim half of high- z proto-clusters should exhibit an enhanced DSFG-rich phase.

While different threads of evidence support both possible explanations – short-lived, bursting proto-clusters or gas-enhanced proto-clusters – measurements of gas depletion times for DSFGs sitting in these structures suggests they are indeed short-lived. Therefore the former evolutionary scenario is favored, where DSFG-rich structures represent a short-lived phase of rapid growth across incredibly large filaments in the IGM. More observations of such structures are needed to constrain the overall population of high- z overdensities, the diversity of their star-formation histories, and to characterize the galaxies within such structures to learn how galaxy growth is governed by environment.

CMC thanks the anonymous referee for helpful comments and the University of Texas at Austin, College of Natural Science for support. CMC also thanks many colleagues for interesting conversations which led up to this paper, including Chao-Ling Hung, Yi-Kuan Chiang, Asantha Cooray, Joel Primack, Amy Barger, Len Cowie, Cedric Lacey, William Cowley, James Bullock, Shea Garrison-Kimmel, Chuck Steidel, and Nick Scoville. CMC would also like to acknowledge financial support and fruitful discussions from the Munich Institute for Astro- and particle Physics (MIAPP) summer programme on the “Star Formation History of the Universe,” held in Munich in August 2015.

REFERENCES

- Andreon, S. *et al.* 2014, A&A, 565, A120.
 Asboth, V. *et al.* 2016, ArXiv e-prints.
 Bahcall, N. A. and Cen, R. 1993, ApJ, 407, L49.
 Bahcall, N. A. *et al.* 2003, ApJ, 585, 182.
 Balestra, I. *et al.* 2010, A&A, 512, A12.
 Balogh, M. L. *et al.* 1998, ApJ, 504(2), 75.
 Barger, A. J. *et al.* 1998, Nature, 394, 248.
 Barger, A. J., Cowie, L. L., and Wang, W.-H. 2008, ApJ, 689, 687.
 Behroozi, P. S., Wechsler, R. H., and Conroy, C. 2013, ApJ, 770, 57.
 Blain, A. W. *et al.* 2004, ApJ, 611, 725.
 Bloemen, J. B. G. M. *et al.* 1986, A&A, 154, 25.
 Bolzonella, M. *et al.* 2010, A&A, 524, A76.
 Bothwell, M. S. *et al.* 2010, MNRAS, 405, 219.
 Bothwell, M. S. *et al.* 2013, MNRAS, 429, 3047.
 Brodwin, M. *et al.* 2007, ApJ, 671, L93.
 Capak, P. *et al.* 2004, AJ, 127, 180.
 Capak, P. L. *et al.* 2011, Nature, 470, 233.
 Carilli, C. L. *et al.* 2011, ApJ, 739, L33.
 Carilli, C. L. and Walter, F. 2013, ARA&A, 51, 105.
 Casey, C. M. 2012, MNRAS, 425, 3094.
 Casey, C. M. *et al.* 2012a, ApJ, 761, 140.
 Casey, C. M. *et al.* 2012b, ApJ, 761, 139.
 Casey, C. M. *et al.* 2009a, MNRAS, 399, 121.
 Casey, C. M. *et al.* 2009b, MNRAS, 395, 1249.
 Casey, C. M. *et al.* 2011, MNRAS, 415, 2723.
 Casey, C. M. *et al.* 2015, ApJ, 808, L33.
 Casey, C. M., Narayanan, D., and Cooray, A. 2014, Phys. Rep., 541, 45.
 Chabrier, G. 2003, PASP, 115, 763.
 Chapman, S. C. *et al.* 2009, ApJ, 691, 560.
 Chapman, S. C. *et al.* 2005, ApJ, 622, 772.
 Chapman, S. C. *et al.* 2004a, ApJ, 606(1), 85.
 Chapman, S. C. *et al.* 2004b, ApJ, 614, 671.
 Chen, C.-C. *et al.* 2013a, ApJ, 762, 81.
 Chen, C.-C. *et al.* 2013b, ApJ.
 Chiang, Y.-K., Overzier, R., and Gebhardt, K. 2013, ApJ, 779, 127.

- Chiang, Y.-K. *et al.* 2015, ApJ, 808, 37.
Christensen, C. R. *et al.* 2015, ArXiv e-prints.
Clements, D. L. *et al.* 2014, MNRAS, 439, 1193.
Collins, C. A. *et al.* 2009, Nature, 458, 603.
Cooper, M. C. *et al.* 2008, MNRAS, 383, 1058.
Cowie, L. L. *et al.* 2004, AJ, 127, 3137.
Cucciati, O. *et al.* 2010, A&A, 524, A2.
da Cunha, E., Charlot, S., and Elbaz, D. 2008, MNRAS, 388, 1595.
Daddi, E. *et al.* 2009, ApJ, 694, 1517.
Dannerbauer, H. *et al.* 2014, A&A, 570, A55.
Diener, C. *et al.* 2015, ApJ, 802, 31.
Doherty, M. *et al.* 2010, A&A, 509, A83.
Dowell, C. D. *et al.* 2014, ApJ, 780, 75.
Downes, D. and Solomon, P. M. 1998, ApJ, 507, 615.
Eisenhardt, P. R. M. *et al.* 2008, ApJ, 684, 905.
Elbaz, D. *et al.* 2007, A&A, 468, 33.
Elbaz, D. *et al.* 2011, A&A, 533, A119+.
Emonts, B. *et al.* 2013, MNRAS, 430(4), 3465.
Flores-Cacho, I. *et al.* 2016, A&A, 585, A54.
Geach, J. E. *et al.* 2005, MNRAS, 363, 1398.
Geach, J. E. *et al.* 2006, ApJ, 649, 661.
Gladders, M. D. and Yee, H. K. C. 2000, AJ, 120, 2148.
Granato, G. L. *et al.* 2015, MNRAS, 450, 1320.
Greve, T. R. *et al.* 2005, MNRAS, 359, 1165.
Grupponi, C. *et al.* 2013, MNRAS, 432, 23.
Hainline, L. J. *et al.* 2011, ApJ, 740, 96.
Hainline, L. J. *et al.* 2009, ApJ, 699, 1610.
Harrison, I. and Coles, P. 2012, MNRAS, 421, L19.
Hatch, N. A. *et al.* 2011, MNRAS, 415, 2993.
Hayashi, M. *et al.* 2012, ApJ, 757, 15.
Hayashino, T. *et al.* 2004, AJ, 128, 2073.
Hayward, C. C. *et al.* 2013, MNRAS, 434, 2572.
Hine, N. K. *et al.* 2016, MNRAS, 455, 2363.
Hinshaw, G. *et al.* 2009, ApJS, 180, 225.
Hodge, J. A. *et al.* 2013a, ApJ, 776, 22.
Hodge, J. A. *et al.* 2013b, ApJ, 768, 91.
Hopkins, A. M. and Beacom, J. F. 2006, ApJ, 651, 142.
Ivison, R. J. *et al.* 2000, ApJ, 542(1), 27.
Ivison, R. J. *et al.* 2013, ApJ, 772, 137.
Kennicutt, Jr., R. C. 1998, ARA&A, 36, 189.
Klypin, A. A., Trujillo-Gomez, S., and Primack, J. 2011, ApJ, 740, 102.
Koyama, Y. *et al.* 2013, MNRAS, 428, 1551.
Kravtsov, A. V. and Borgani, S. 2012, ARA&A, 50, 353.
Kubo, M. *et al.* 2015, ApJ, 799, 38.
Kuiper, E. *et al.* 2011, MNRAS, 415, 2245.
Kurk, J. D. *et al.* 2004, A&A, 428, 817.
Kurk, J. D. *et al.* 2000, A&A, 358, L1.
Lacey, C. G. *et al.* 2015, ArXiv e-prints.
Le Fèvre, O. *et al.* 2005, A&A, 439, 845.
Lee, K.-G. *et al.* 2016, ApJ, 817, 160.
Lee, K.-S. *et al.* 2014, ApJ, 796, 126.
Lehmer, B. D. *et al.* 2009, MNRAS, 400, 299.
Lewis, I. *et al.* 2002, MNRAS, 334, 673.
Lilly, S. J. *et al.* 2009, ApJS, 184, 218.
Lindner, R. R. *et al.* 2011, ApJ, 737, 83.
Marconi, A. *et al.* 2004, MNRAS, 351, 169.
Martini, P. 2004, Coevolution of Black Holes and Galaxies, 169.
Matsuda, Y. *et al.* 2005, ApJ, 634, L125.
Menanteau, F. and Hughes, J. P. 2009, ApJ, 694, L136.
Miley, G. K. *et al.* 2004, Nature, 427, 47.
Miller, T. B. *et al.* 2015, MNRAS, 452, 878.
Mo, H. J. and White, S. D. M. 1996, MNRAS, 282, 347.
Muldrew, S. I., Hatch, N. A., and Cooke, E. A. 2015, MNRAS, 452, 2528.
Narayanan, D. *et al.* 2015, Nature, 525, 496.
Newman, A. B. *et al.* 2014, ApJ, 788, 51.
Noble, A. *et al.* 2013, ApJ, 768, 118.
Oñorbe, J. *et al.* 2014, MNRAS, 437, 1894.
Oliver, S. J. *et al.* 2012, MNRAS, 424, 1614.
Palunas, P. *et al.* 2004, ApJ, 602, 545.
Patel, S. G. *et al.* 2009, ApJ, 705, L67.
Peacock, J. A. 1999, Royal Society of London Philosophical Transactions Series A, 357, 133.
Planck Collaboration *et al.* 2013, A&A, 550, A131.
Planck Collaboration *et al.* 2015, A&A, 582, A30.
Popesso, P. *et al.* 2009, A&A, 494, 443.
Press, W. H. and Schechter, P. 1974, ApJ, 187, 425.
Reddy, N. *et al.* 2012, ApJ, 744, 154.
Reddy, N. A. and Steidel, C. C. 2009, ApJ, 692, 778.
Reddy, N. A. *et al.* 2006, ApJ, 653, 1004.
Rigby, E. E. *et al.* 2014, MNRAS, 437, 1882.
Rosati, P., Borgani, S., and Norman, C. 2002, ARA&A, 40, 539.
Scoville, N. *et al.* 2013, ApJS, 206, 3.
Scoville, N. *et al.* 2014, ApJ, 783, 84.
Scoville, N. *et al.* 2015, ApJ, 800, 108.
Seymour, N. *et al.* 2012, ApJ, 755, 146.
Sheth, R. K., Mo, H. J., and Tormen, G. 2001, MNRAS, 323, 1.
Shimasaku, K. *et al.* 2003, ApJ, 586, L111.
Silverman, J. D. *et al.* 2008, ApJ, 679, 118.
Simpson, J. M. *et al.* 2014, ApJ, 788, 125.
Skibba, R. A. *et al.* 2009, MNRAS, 399, 966.
Smail, I., Ivison, R. J., and Blain, A. W. 1997, ApJ, 490, L5+.
Solomon, P. M. *et al.* 1987, ApJ, 319, 730.
Solomon, P. M. and Sage, L. J. 1988, ApJ, 334, 613.
Spitler, L. R. *et al.* 2012, ApJ, 748, L21.
Springel, V. 2005, MNRAS, 364, 1105.
Steidel, C. C. *et al.* 1998, ApJ, 492, 428.
Steidel, C. C. *et al.* 2005, ApJ, 626, 44.
Steinhardt, C. L. *et al.* 2015, ArXiv e-prints.
Stevens, J. A. *et al.* 2003, Nature, 425, 264.
Subramanian, K. and Swarup, G. 1992, Nature, 359, 512.
Swinbank, A. M. *et al.* 2014, MNRAS, 438, 1267.
Tamura, Y. *et al.* 2009, Nature, 459, 61.
Tanaka, I. *et al.* 2011, PASJ, 63, 415.
Toft, S. *et al.* 2014, ApJ, 782, 68.
Umehata, H. *et al.* 2015, ApJ, 815, L8.
van der Burg, R. F. J., Hildebrandt, H., and Erben, T. 2010, A&A, 523, A74.
van der Burg, R. F. J. *et al.* 2013, A&A, 557, A15.
Vanderlinde, K. *et al.* 2010, ApJ, 722, 1180.
Venemans, B. P. *et al.* 2002, ApJ, 569, L11.
Venemans, B. P. *et al.* 2005, A&A, 431, 793.
Venemans, B. P. *et al.* 2007, A&A, 461, 823.
Vogelsberger, M. *et al.* 2014, MNRAS, 444, 1518.
Wake, D. A. *et al.* 2005, ApJ, 627, 186.
Walter, F. *et al.* 2012, Nature, 486, 233.
Webb, T. M. A. *et al.* 2013, AJ, 146, 84.
Wechsler, R. H. *et al.* 2002, ApJ, 568, 52.
Weiß, A. *et al.* 2009, ApJ, 705, L45.
Wirth, G. D. *et al.* 2004, AJ, 127, 3121.
Yamada, T. *et al.* 2012, AJ, 143, 79.
Yuan, T. *et al.* 2014, ApJ, 795, L20.